Fusion of IVUS and OCT Through Semi-Automatic Registration

Gozde Unal[1], Shawn Lankton[1], Stephane Carlier[2,3], Greg Slabaugh[1], and Yunqiang Chen[1]

[1] Siemens Corporate Research, Princeton, NJ, USA gozde.unal@siemens.com
[2] Department of Medicine-Cardiology, Columbia University, New York, USA
[3] Cardiovascular Research Foundation, New York, USA ⋆

Abstract. The most frequent cause of heart attack and sudden cardiac death is the disruption of plaque build ups in the arteries. Current technologies such as intravascular ultrasound (IVUS) and optical coherence tomography (OCT) image the vessels from inside-out in order to detect plaque deposits as well as other structures. In this work we develop a novel image fusion technique that produces images with greater quality and quantity of information by establishing a correspondence between the two modalities. We employ a three step process using feature extraction, registration, and image fusion. The final results of our algorithm represent an improvement over each modality individually.

1 Introduction

The fusion of different medical image modalities is a clinically welcomed procedure for providing physicians with more enhanced diagnostic information and computer algorithms with higher resolution, richer image measurements. This fusion would not be possible without multi-modal image registration, which is now an essential tool in medical imaging.

The purpose of this paper is to develop a novel image fusion of intravascular ultrasound (IVUS) and optical coherence tomography (OCT) images to aid the study of atherosclerotic plaques. Atherosclerosis is a disease characterized by a deposit of plaque in arterial wall over time. The disruption of an atherosclerotic plaque is considered to be the most frequent cause of heart attack and sudden cardiac death [1]. Therefore, studying vulnerable plaques constitutes a major research area in the field of clinical and medical imaging. Merging imaging techniques will advance the diagnostic accuracy of IVUS and OCT and might improve the detection of rupture-prone plaques.

Intravascular ultrasound (IVUS) is a widely available clinical tool for guiding percutaneous interventions. (See Figure 1-b) While IVUS uses frequencies from 20 to 40 MHz and provides good penetration depth, it lacks high enough accuracy (resolution 120μm) to study thin-cap atheroma lesions. Optical coherence tomography (OCT) is a newer imaging modality that provides high resolution (15-20μm) tomographic visualization of coronary arteries (see Figure 1-c). However, OCT lacks penetration with a maximum of only 1-2 mm into the plaque, but it can image behind calcifications clearly while ultrasounds are intensely reflected. The current high resolution capabilities of OCT are well suited for imaging vulnerable plaques but poor depth penetration hamper full characterization of coronary lesions and plaque burden. Since IVUS penetrates

⋆ We thank Joe Schmitt, Chenyang Xu from Light Lab Imaging, and Amin Katouzian from Columbia University for their help in data collection and import.

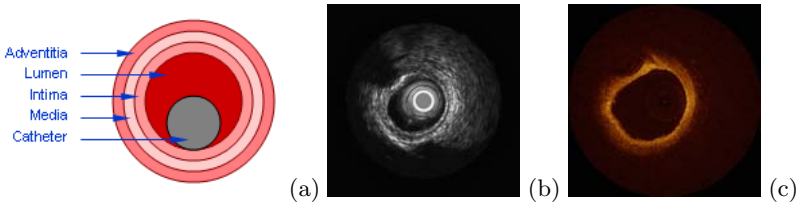

Fig. 1. Anatomy of vessel (a), IVUS image with catheter artifacts (b), OCT image (c).

deeper into the media and adventitia, combining OCT and IVUS modalities will enhance quantitative analysis of coronary arteries significantly (see Figure 1-a for a diagram of vessel anatomy).

Multi-modal image registration techniques have been presented among various imaging modalities: Magnetic Resonance (MR) and Computed Tomography (CT) images, Ultrasound and CT, PET and CT, and so on. Multi-modal image registration through information theoretic measures, such as mutual information [2, 3], Kulback-Liebler divergence, and other similarity metrics [4] have been extremely popular for both rigid and non-rigid registration. In two main streams of registration, landmark-based approaches utilize a set of fiducial marks, either automatically extracted or selected by the user [5, 6], whereas image intensity-based registration approaches utilize global or local image matching metrics such as cross-correlation and sum of squared differences [7–9]. See surveys [10, 11].

Our contribution in this paper is to develop a computer assisted image fusion of IVUS and OCT by a two phase registration. The practical advantage of fusion is to make use of deep penetration of IVUS in addition to the high resolution of OCT for imaging of the plaque. Our method is currently semi-automatic due to user selection of key image frames from each of the IVUS and OCT datasets to bypass longitudinal registration in 3D, which will be addressed in a future work. Instead we focus on the transverse plane registration of the 2D image frames. To our knowledge, this is the first study that fuses the two intravascular imaging modalities, IVUS and OCT. Our hypothesis is that combining these images will improve the accuracy of plaque characterization and further studies of vulnerable plaque via finite element modeling and fluid structure interaction.

2 Method

In this section, we explain the steps of our IVUS-OCT fusion method. Our assumption is that the longitudinal correspondence of input pairs from IVUS and OCT pullback volumes are selected manually by the user, and the developed method handles the automatic transverse plane registration afterwards.

We combine a landmark-based rigid registration method with an image-based non-rigid registration in order to align and fuse the IVUS and OCT modalities. As such our approach is comprised of several steps: i.) extracting landmarks in the different datasets, and establishing the correspondence between them; ii.) estimating the rigid transformation between the datasets using the landmarks; iii.) aligning the two datasets further by non-rigid registration; iv.) fusing the two datasets using the computed transformations. The above steps are explained in the next subsections.

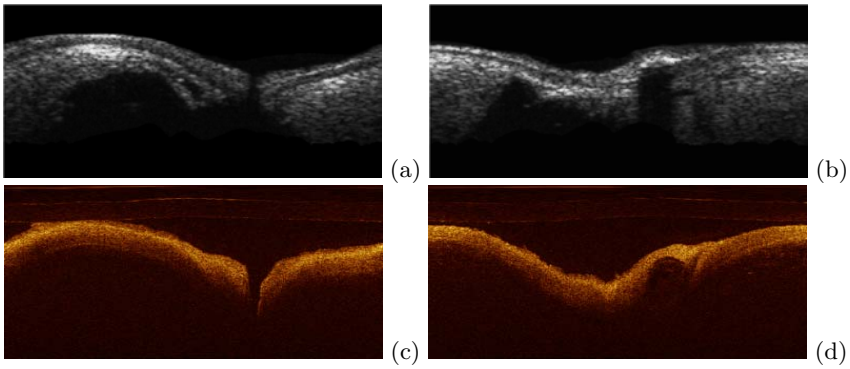

Fig. 2. Side Branch in IVUS (a) and OCT (c), Calcification in IVUS (b) and OCT (d).

2.1 Feature Extraction

Landmarks can take the form of points, lines, surfaces, or volumes. We chose to utilize landmarks in the form of contours that will provide correspondence between IVUS and OCT image data. When determining the location of these contours all of our computations are carried out in a rectangular format, which is the original acquisition format.

The important features we use to create these contours are the inner arterial wall, the side branches, and the calcification regions. Our algorithm works on matched pairs of 2D key frames from corresponding scans that contain a side branch, a large calcification region, or both. First, the inner wall of the vessel is segmented using a previously developed segmentation algorithm [12]. Once this is complete, the detection of side branches and calcification regions can begin.

Side branches are identified as the openings formed when the vessel being imaged bifurcates. This is visualized as an area of dark intensity extending from the lumen in the near field towards the far field (Figure 2-a and 2-c). The intensity pattern is detectable in the rectangular image domain as a dark intensity segment extending in the radial direction (vertically in the rectangular image).

Calcium deposits are places along the vessel wall where minerals have collected to form dense pockets. In IVUS, these deposits can be recognized by the presence of a bright echo along the lumen and shadowing of the far-field structures. This distinctive pattern is observed in OCT (Figure 2-b and 2-d). The intensity pattern used to identify these features is a dark inclusion delimited by sharp borders without shadowing.

In order to detect these features the thickness of the detected vessel wall is measured over the entire scan. This is accomplished by first extracting a contour that traces the farthest-field data that was obtained. In the rectangular domain, this corresponds to the bottom of the grayscale data. Next, the segmented lumen contour is projected outward radially by a small distance. This distance is set adaptively based on the average thickness of the imaged vessel. Typically, IVUS images use a larger distance than OCT images due to innate differences in the technologies. In Figure 3 the farthest-field contour is marked in white while the projection of the lumen contour is displayed in blue for both images.

A measure for thickness is obtained by computing the distance between the projected lumen contour and the detected contour representing the farthest-

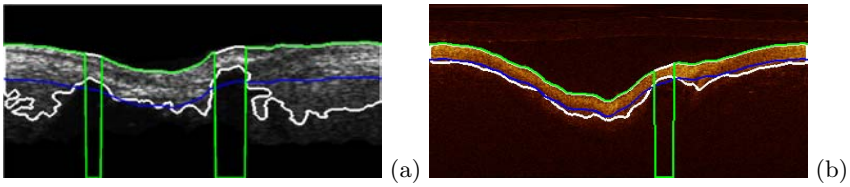

Fig. 3. Segmented pair showing all possible feature locations. IVUS (a), OCT (b).

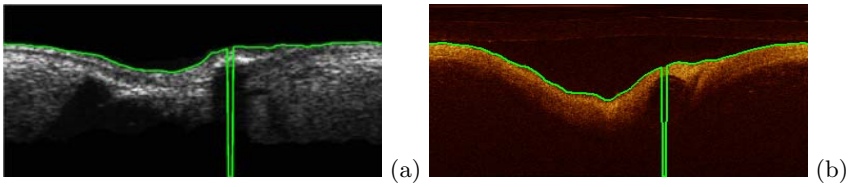

Fig. 4. Final feature detector output in the rectangular domain. IVUS (a), OCT (b).

field structures. Places where the farthest-field structures are either missing or extremely close to the lumen contour represent possible feature locations. In Figure 3 feature locations are marked by vertical green lines.

Once feature locations have been identified, they are examined in more detail. Locations which have a significantly darker lumen in the feature area are classified as branches while locations which have particularly bright lumen in the feature area are classified as calcifications. If the intensity of the lumen in the feature area is not significantly high or low the feature is assumed to be incorrectly labeled and is discarded.

In the registration phase it is simpler to use the single most distinctive feature. Thus, the feature contour is analyzed once more. If a branch is present it is used. If no branches are present then the calcification which formed the most intense shadows (and therefore thinnest detected contour) is used. A contour tracing the inner boundary of the lumen and extending sharply into the far field at the center of the feature is created as the final feature detection output. Figure 4 Shows the final result of the feature extraction after post processing. These contours are then transformed back to the polar display domain where the registration step takes place.

2.2 Rigid Registration Based on Feature Maps

In order to solve the correspondence problem from IVUS to OCT we need to register the feature contours built in the previous section. Because OCT is the higher resolution imaging modality the IVUS image will be deformed to align with the OCT image. The correspondence is found very naturally by embedding the contours $\boldsymbol{C} \in \Omega$ in the image domain $\Omega \in \mathbb{R}^2$ implicitly as the zero-level set of a signed distance function $\Phi : \mathbb{R}^2 \longrightarrow \Omega$:

$$\boldsymbol{C} = \{(x, y) \in \Omega | \Phi(x, y) = 0\}. \tag{1}$$

This representation, which eases the rigid registration step, can be directly plugged into a sum of squared differences (SSD) criterion:

$$SSD(\boldsymbol{g}) = \int_{\Omega} (\Phi^i(\boldsymbol{g}(x, y)) - \Phi^o(x, y))^2 dxdy, \tag{2}$$

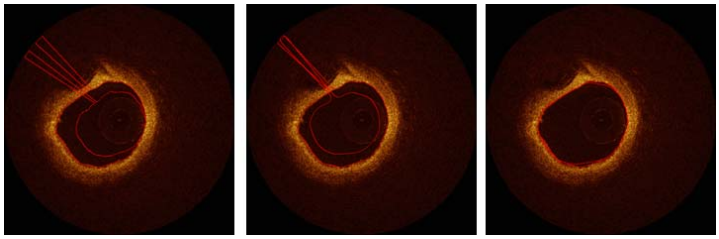

Fig. 5. Several selected iterations taken during rigid registration.

where the unknown g is a rigid motion in $\mathbb{R}^2$ to be estimated, and the superscripts ^{i} and ^{o} denote the IVUS and the OCT images, respectively. The rigid motion $\boldsymbol{g} : \mathbb{R}^2 \longrightarrow \mathbb{R}^2$ has 2 translation parameters, a rotation parameter and a scale parameter. The rigid registration equation for each transformation parameter g_i is derived from the cost functional above by taking its first variation:

$$\frac{\partial g_i}{\partial t} = \oint_{\boldsymbol{C}^i} (\Phi^i(\boldsymbol{g}\,(x,y)) - \Phi^o(x,y)) < \nabla\Phi^i, \frac{\partial g_i}{\partial p} > dp, \tag{3}$$

Here p denotes a uniform parameter on the contour $\boldsymbol{C}^i$. With the level set representation, and a simple finite differencing discretization of the Eq.(3), a simulated rigid motion can be extracted. Figure 5 shows several steps in the evolution of the rigid registration of two feature contours.

2.3 Non-Rigid Registration for Refinement

After rigid registration, we perform a non-rigid registration to account for local deformations between the IVUS and OCT images. The vector field $\boldsymbol{u} : \Omega \longrightarrow \Omega$ that represents the discrete displacement field from the already rigidly transformed IVUS image $I^{i,R}$ to the OCT image I^o will be estimated by a minimization of a similarity metric between some appropriately processed and transformed image intensity functions. In a multi-modal image registration, image intensities usually can not be used for alignment directly and should be transformed according to the application. In IVUS and OCT image modalities image intensity patterns are very different, but the strong gradients on and around the dominant structures are naturally very similar. Therefore, a highly smoothed gradient image is used as a similarity metric for image matching.

We chose the normalized cross correlation as a statistical similarity measure for a non-rigid alignment: $CC(\boldsymbol{u}\,) = \frac{\mathrm{cov}(I^{i,R}(\boldsymbol{x}+\boldsymbol{u}\,(\boldsymbol{x}\,))-I^o(\boldsymbol{x}\,))}{\sqrt{\mathrm{var}(I^{i,R}(\boldsymbol{x}+\boldsymbol{u}\,(\boldsymbol{x}\,)))\ \mathrm{var}(I^o(\boldsymbol{x}\,))}}$ where cov denotes the covariance of the intensities between $I^{i,R}(\boldsymbol{x}\,)$ and $I^o(\boldsymbol{x}\,)$, and var denotes the variance of the intensities in an image. In order to regularize the unknown vector field $\boldsymbol{u}\,$, a penalty on its variation is added.

$$CC(\boldsymbol{u}\,) = \frac{\mathrm{cov}(I^{i,R}(\boldsymbol{x}\,+\boldsymbol{u}\,(\boldsymbol{x}\,)) - I^o(\boldsymbol{x}\,))}{\sqrt{\mathrm{var}(I^{i,R}(\boldsymbol{x}\,+\boldsymbol{u}\,(\boldsymbol{x}\,)))\ \mathrm{var}(I^o(\boldsymbol{x}\,))}} + \int_\Omega ||\nabla\boldsymbol{u}\,||^2 d\boldsymbol{x} \tag{4}$$

This encourages a smoothly varying vector field. A variational approach to derive the above cost functional results in partial differential equations to estimate the displacement field $\boldsymbol{u}$ (see [13] for the final equations).

2.4 Fusion

The final step of our algorithm is to fuse the two aligned images $I^{i,R,N}$ and I^o. The two modalities IVUS and OCT will be fused in a weighted way based on prior anatomical information and strengths of each modality. Calcium has well-defined borders in OCT images, particularly for the first 2 mm, and appears as a shadow behind a bright echo in IVUS images. Thus, the two modalities will be fused through a convex combination, which is spatially weighted according to the distance from the lumen boundary. In the first 2 mm from the edge of the lumen contour, only OCT data is shown. Over the next 1 mm a linear transition occurs where the OCT weight is decreased to zero as IVUS weight is increased. Farther than 3mm from the lumen contour, only IVUS data is shown.

3 Results and Conclusions

Our results have been summarized in Figure 6: the fused images represent an enhancement in the amount of information contained in each frame. As a result, improved diagnostic accuracy of plaque characteristics and further analysis of arterial wall properties can be accomplished.

This novel image fusion technique has been shown to be capable of combining information contained in IVUS and OCT imagery and producing new images which present all relevant information in a more convenient form. The final fusion results display the highly accurate, but shallow penetrating OCT data when available and seamlessly blend into the less accurate, but far reaching IVUS data. This will facilitate identification of detailed near-field structures such as thin-cap atheroma lesions as well as the deeper structures to assess the plaque burden or the remodeling index of coronary lesions. Thus using this type of visualization will allow physicians to make higher quality diagnoses in less time.

One current limitation of this technique is that it requires that matched frames with discernable features be provided by a user. However, the algorithms developed in this study will be extremely useful in extending the results obtained here to future work. We plan to eventually create fusion/compound imaging automatically from the IVUS and OCT pull-back volumes in 3D. Transverse plane registration of key frames will be a key component in producing a high resolution 3D mesh structure of the arterial wall showing locations of coronary plaques.

References

1. Fuster, V., Moreno, P., Fayad, Z., Corti, R., Badimon, J.: Atherothrombosis and high-risk plaque: part I: Evolving concepts. J. Am. Coll. Cardiol. **46**(6) (2005) 937–954
2. Wells, W., Viola, P., Atsumi, H., Nakajima, S., Kikinis, R.: Multi-modal volume registration by maximization of mutual information. Medical Image Analysis **1** (1996) 35–51
3. Maes, F., Collignon, A., Vandermeulen, D., Marchal, G., Suetens, P.: Multi-modality image registration by maximization of mutual information. IEEE Trans. Med. Imaging **16** (1997) 187–198
4. Leventon, M., Grimson, E.: Multi-modal volume registration using joint intensity distributions. In: MICCAI-Springer-Verlag. (1998) 1057–1066
5. Joshi, S., Miller, M.I.: Landmark matching via large deformation diffeomorphisms. IEEE Trans. Image Process. **9**(8) (2000) 1357–1370

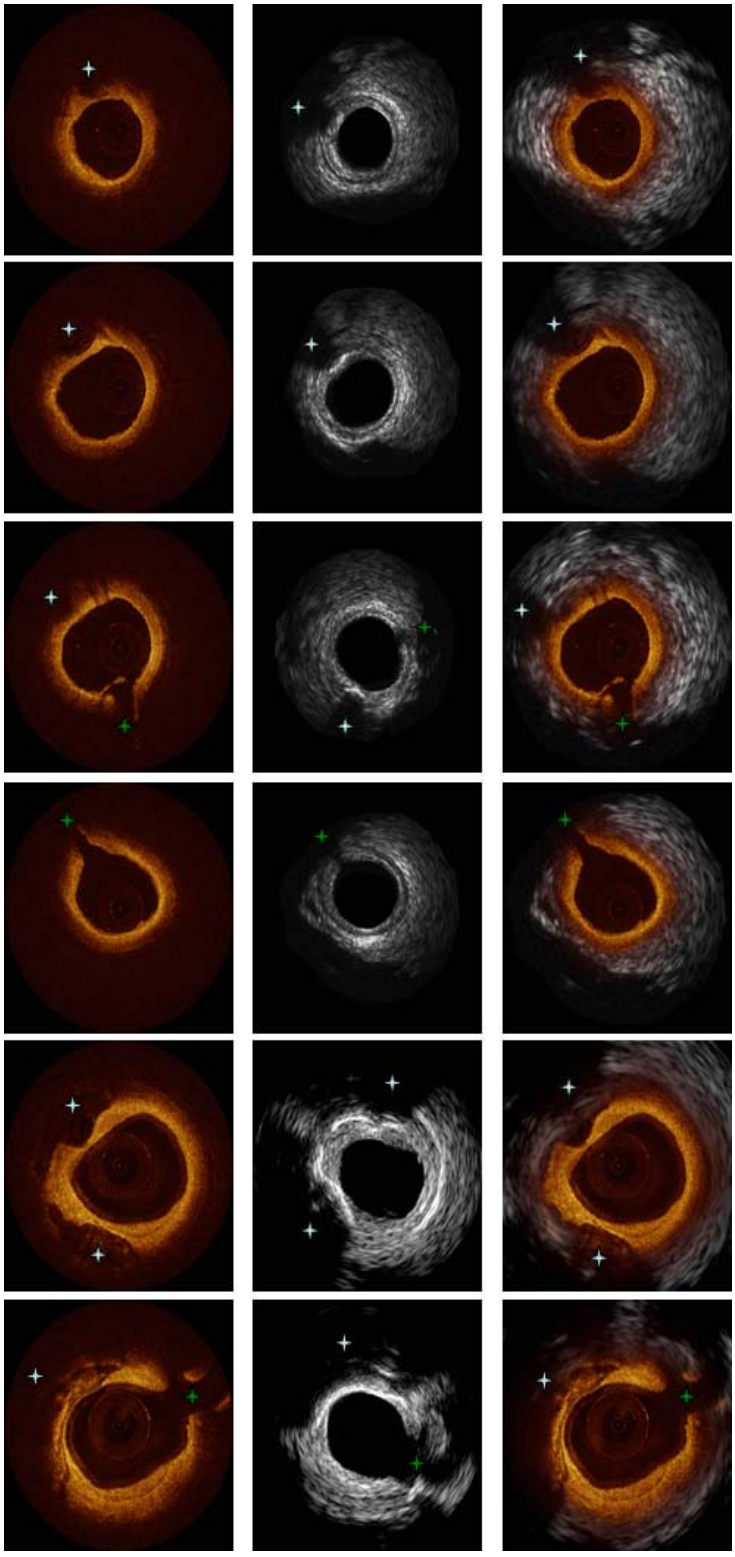

Fig. 6. Fusion results from six matched key frames. The columns show OCT images, matched IVUS images, and the fused result after registration respectively. The fiducial markings were placed manually to illustrate which primary features were aligned during rigid registration. Blue indicates a calcification, and green indicates a side branch.

6. Rohr, K., Stiehl, H., Sprengel, R., Buzug, T., Weese, J., Kuhn, M.: Landmark-based elastic registration using approximating thin-plate splines. IEEE Trans. on Medical Imaging **20**(6) (2001) 526–534
7. Alvarez, L., Weickert, J., Sánchez, J.: Reliable estimation of dense optical flow fields with large displacements. International Journal of Computer Vision **39**(1) (2000) 41–56
8. Christensen, G.E., Rabbitt, R.D., Miller, M.I.: Deformable templates using large deformation kinematics. IEEE Trans. Image Process. **5**(10) (1996) 1435–1447
9. Chefd'hotel, C., Hermosillo, G., Faugeras, O.: A variational approach to multi-modal image matching. In: VLSM Workshop-ICCV. (2001) 21–28
10. Maintz, J., Viergever, M.: A survey for medical image registration. Medical Image Analysis **2**(1) (1998) 1–36
11. Pluim, J., Maintz, J., Viergever, M.: Mutual-information-based registration of medical images: A survey. IEEE Trans. Medical Imaging **22** (2003) 986–1004
12. Unal, G., Bucher, S., Carlier, S., Slabaugh, G., Fang, T., Tanaka, K.: Shape-driven segmentation of intravascular ultrasound images. In: MICCAI-CVII The 1st International Workshop on Computer Vision for Intravascular and Intracardiac Imaging. (2006)
13. Hermosillo, G., Chefd'Hotel, C., Faugeras, O.: Variational methods for multi-modal image matching. International Journal of Computer Vision **50** (2002) 329–343